Hydrogen purification over lanthanum-doped iron oxides by WGSR

Maria do Carmo Rangel[a,b,*], Peterson Santos Querino[a], Sarah Maria Santana Borges[a],
Sergio Gustavo Marchetti[c], José Mansur Assaf[d], Doris Polett Ruiz Vásquez[e],
Cristiane Barbieri Rodella[f], Tatiana de Freitas Silva[d], Alisson Henrique Marques da Silva[d],
Adriana Paula Ramon[d]

[a] Instituto de Química, Universidade Federal da Bahia, Campus Universitário de Ondina, Federação, 40 170-280, Salvador, Bahia, Brazil
[b] Instituto de Química,Universidade Federal do Rio Grande do Sul, Av. Bento Gonçalves, 9500, Agronomia, 90650-001 Porto Alegre, RS, Brazil
[c] CINDECA, Facultad de Ciencias Exactas, Universidad Nacional de La Plata, 1900, 47 y 115 La Plata, Argentina
[d] Universidade Federal de São Carlos, Rod. Washington Luiz, Km 235, 13565-905, São Carlos, São Paulo, Brazil
[e] Facultad de Ciencias Químicas, Universidad de Concepción, Casilla 3-C, Concepción, Chile
[f] Brazilian Center for Research in Energy and Materials (CNPEM) – Brazilian Synchrotron Light Laboratory (LNLS), C. P. 6192, 13083-970, Campinas, SP, Brazil

ARTICLE INFO

ABSTRACT

Hydrogen technology has been greatly increased in last decades as a promising solution to protect the environment. When carbon-based feedstocks are used, such as natural gas, biomass and biogas, the water gas shift reaction (WGSR) plays an important step in the production of high pure hydrogen for several purposes. By this reaction, the residual carbon monoxide in the gaseous stream (coming from steam reforming of carbon-based feedstocks) can be converted to carbon dioxide and then removed from the stream, avoiding the poisoning of industrial metallic catalysts as well as of electrocatalysts in fuel cells. Aiming to obtain no toxic catalysts that can replace the commercial chromium-doped hematite catalysts, lanthanum-doped hematite was studied in this work. Iron oxide-based samples with different amounts of lanthanum (La/Fe (molar) = 0.02; 0.08 and 0.2) were obtained by sol-gel method and calcined at 600 °C. The catalysts were characterized by X-ray diffraction, specific surface area measurements, temperature programmed reduction, Raman spectroscopy, Mössbauer spectroscopy, transmission electron microscopy and X-ray photoelectron spectroscopy. It was found that lanthanum affected the textural and reducing properties of hematite, depending on the amount. Moreover, lanthanum oxide increased the activity of hematite by decreasing the size of hematite crystals and then increasing the number of exposed active sites. In addition, lanthanum favored hematite reduction to produce magnetite (active phase). The activity increased with the amount of lanthanum in solids, the lanthanum-richest sample being the most active catalyst.

1. Introduction

In last decades, hydrogen has been pointed out as one of the most attractive alternatives to fossil fuels to reduce greenhouse gas emissions and to meet the increasing energy demand worldwide. Hydrogen has unique physical and chemical properties so that it has found several applications as fuel and as feedstock for chemical, food and refining industries, besides in the steel and electronics industries [1]. Hydrogen has also the advantages of being efficient, cost attractive and a clean burning fuel, which can be stored as a liquid or gas [2,3]. However, hydrogen is not available in nature and then should be produced by any primary energy source fossil or renewable [2,4].

Despite the current energy sources must meet the requirements of being carbon-free and renewable, most of commercial hydrogen is still produced from natural gas, through the different reforming processes (steam reforming, partial oxidation, dry reforming or autothermal reforming) [3–6]. For all reforming processes, a hydrogen-rich gaseous mixture containing different amounts of carbon monoxide, carbon dioxide, steam and unreacted methane is produced, depending on the type of reforming process [5]. However, the presence of carbon monoxide in hydrogen-rich streams is highly undesirable since it can irreversibly poison most of metallic catalysts used in chemical processes [7,8] as well as the platinum electrocatalysts in proton exchange membrane fuel cell (PEMFC), an important technology for producing clean energy [9]. Therefore, carbon monoxide should be removed from the stream by an efficient and economical way. The water gas shift

reaction (WGSR) fits these requirements and thus has been widely used as an additional step just after the reforming stage, in the commercial production of high pure hydrogen [7]. The reaction is also largely used to adjust the hydrogen to carbon monoxide molar ratio in several industrial processes such as methanol synthesis and Fischer-Tropsch reaction [7,10].

In spite of the great reserves of natural gas worldwide and the expectation that its use will continue to expand in the future [11], the share of renewable technologies is expected to increase in the near future [12–15]. Therefore, a lot of work have been devoted to hydrogen production from renewable sources, including biomass [6] and biogas [16], among others. While biogas can produce hydrogen by reforming processes, especially by dry reforming [6,16], the thermochemical and biological methods are the main routes for hydrogen production from biomass [6]. Biological processes are performed under mild conditions and then are more environmentally benign and less energy intensive, but generally low rates and yields of hydrogen are obtained [17]. On the other side, thermochemical processes, especially pyrolysis and gasification, are more suitable to commercial applications, since it is much faster and provide higher yields of hydrogen. From both pyrolysis and gasification, methane and carbon monoxide are produced, which can be further processed to produce more hydrogen, by reforming processes and WGSR [6]. Therefore, WGSR is expected to play an important role in biorefineries in the future.

The WGSR (Eq. (1)) is exothermic and reversible and then favored by low temperatures and large amounts of steam. This requires two steps in industrial operations to achieve high conversions for commercial purposes. In the first one (HTS, High Temperature Shift), the reaction is performed under favorable kinetic conditions in the range of 350–420 °C, over iron-based (e.g., Fe/Cr) catalysts. The following stage (LTS, Low Temperature Shift) is carried out under favorable thermodynamics conditions in the range of 200–250 °C, over copper-based (e.g., Cu/Zn/Al) catalysts [7,8,10,18].

$$CO_{(g)} + H_2O_{(g)} \rightleftarrows CO_{2(g)} + H_{2(g)} \ \Delta H° = -41.2 \ kJ \ mol^{-1}$$
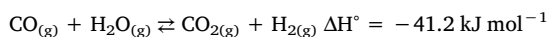
Over the years, the HTS step has been performed over catalysts based on chromium-doped iron oxides, which show several advantages such as low cost, thermal stability and resistance against poisons [7,10,19]. They are normally sold as hematite (α-Fe_2O_3) and should be reduced in situ to produce magnetite (Fe_3O_4) which is the active phase. In recent years, these catalysts were improved by the addition of copper, which acts as an electronic promoter [19,20]. On the other hand, the role of chromium oxide (Cr_2O_3) is to avoid the loss of specific surface area of the catalyst during operation, acting as a textural promoter [7,10,21]. Despite of these advantages, several studies have been addressed to replace chromium by other dopants [8,9,19,20,22] as well as to find alternative catalysts for WGSR [23–27], because of the carcinogenic nature of chromium compounds.

Aiming to find alternative dopants to hematite-based catalysts for WGSR, the effect of lanthanum on the properties of iron oxides was studied in this work. The improvement of the textural properties of hematite by lanthanum was previously demonstrated for catalysts active in styrene production [13].

2. Experimental

2.1. Catalyst preparation

Samples based on lanthanum-doped hematite (α-Fe_2O_3) with different amount of lanthanum (La/Fe (molar) = 0.02, 0.08 and 0.2) were obtained by the sol-gel method.

The poorest-lanthanum sample (La/Fe = 0.02) was prepared by the addition of 250 mL of ferric nitrate (1 mol L^{-1}), lanthanum nitrate (0.02 mol L^{-1}) and ammonium hydroxide (28%) solutions to a beaker containing water, using a peristaltic pump under stirring, at room
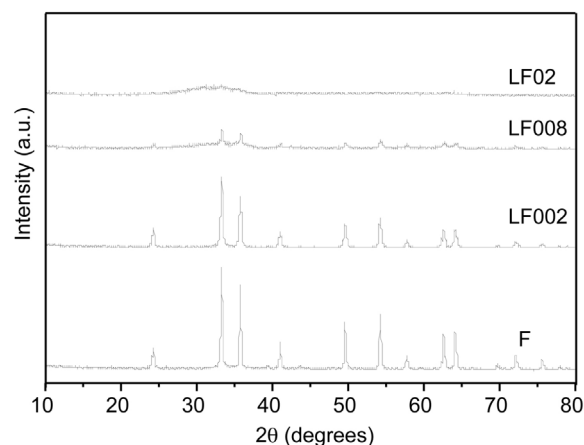
(a)
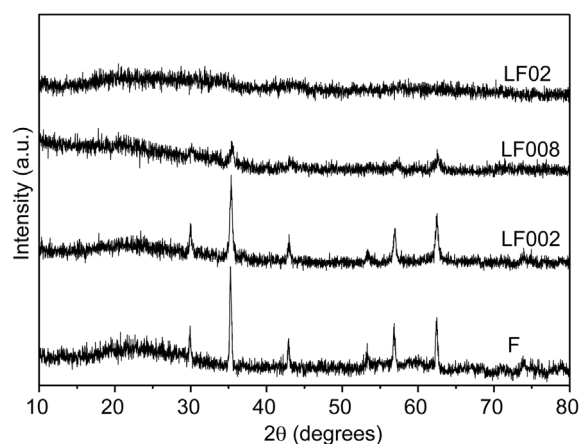
(b)

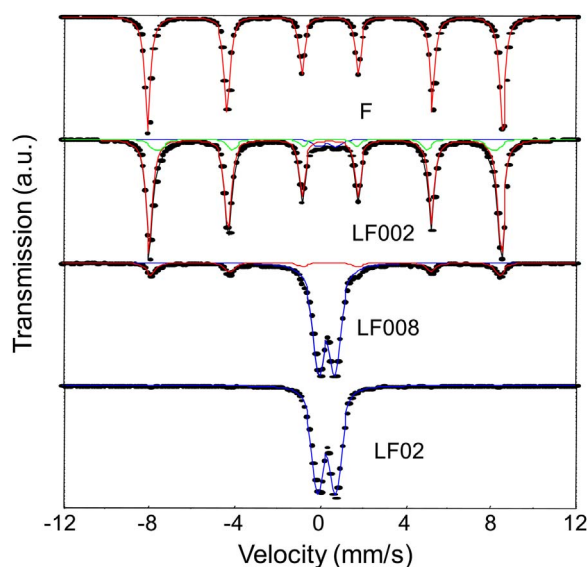**Fig. 1.** X-ray diffractograms for the fresh (a) and spent (b) catalysts.

Fig. 2. Mössbauer spectra at 25 °C for the fresh catalysts.

temperature. After the complete addition of the reactants (pH = 10), the system was kept under stirring for additional 30 min and then centrifuged (2000 rpm, 4 min) to obtain a gel, which was washed with water and centrifuged again. The gel was washed and the sol

Table 1
Mössbauer parameters for fresh catalysts at 25 °C.

Species	Parameters	F	LF002	LF008	LF02
α-Fe$_2$O$_3$	H (T)	51.52 ± 0.01	51.08 ± 0.01	50.66 ± 0.05	–
	δ (mm/s)	0.37 ± 0.01	0.37 ± 0.01	0.38 ± 0.01	–
	2ε (mm/s)	−0.22 ± 0.01	−0.22 ± 0.01	−0.24 ± 0.01	–
	%	100	84 ± 4	80 ± 1	–
α-Fe$_2$O$_3$ with small size[a]		–	48.9 ± 0.6	–	–
		–	0.37 ± 0.01	---	–
		–	−0.18 ± 0.02	–	–
		–	13 ± 4	–	–
(P) Fe^{3+} or (SP) α-Fe$_2$O$_3$	δ (mm/s)	–	0.36 ± 0.03	0.34 ± 0.01	0.33 ± 0.01
	Δ (mm/s)	–	0.82 ± 0.04	0.76 ± 0.01	0.84 ± 0.01
	%	–	3 ± 1	20 ± 1	100

H: hyperfine magnetic field in Tesla; δ: isomer shift (all the isomer shifts are referred to α-Fe at 25 °C); 2ε: quadrupole shift; Δ: quadrupole splitting; (P): paramagnetic species; (SP): superparamagnetic species.

[a] Hyperfine parameters of the sextuplet assigned to α-Fe$_2$O$_3$ with small size corresponds to the species that show magnetic collective excitations.

Table 2
Average crystals diameter calculated by the collective magnetic excitations model.

| Sample	H$_{obs}$(T)	D (nm)
F	51.52	93
LF002	51.08–48.9	62–37
LF008	50.66	52

centrifuged until nitrate ions were no longer detected in the supernatant. These species were identified by adding 1 mL of concentrated sulfuric acid to about 10 mL of the supernatant [28]. The obtained gel was dried in an oven at 120 °C for 24 h, ground and sieved in 100 mesh. Then the solid was heated (10 °C min^{-1}) under nitrogen flow up to 600 °C and kept at this temperature for 2 h to produce the LF002 sample (La/Fe = 0.02). The LF008 and LF02 samples (La/Fe = 0.08 and 0.2) were obtained using the same procedure but using 0.08 mol L^{-1} and 0.2 mol L^{-1} in lanthanum nitrate, respectively. Samples of pure iron oxide (F sample) and pure lanthanum oxide (L) were also obtained, which were used as References

2.2. Catalyst characterization

The catalysts were characterized by X-ray diffraction (XRD), specific surface area (Sg) measurements, temperature programmed reduction (TPR), Raman spectroscopy, Mössbauer spectroscopy, X-ray photoelectron spectroscopy (XPS), transmission electron microscopy (TEM) and electron diffraction (ED).

The X-ray diffraction experiments were carried out in a Shimadzu XRD-6000 model equipment using a CuKα radiation (λ = 1.54059 Å) generated at 40 kV and 30 mA and a nickel filter. The diffractograms were registered at room temperature, using a scanning velocity of 2° min^{-1} in the range of 10–80° (2θ). For the specific surface areas measurements, the nitrogen adsorption at −196 °C and the BET model were used in a Micromeritics ASAP 2020 instrument. Before analysis, the sample (0.5 g) was heated up to 200 °C under vacuum in order to remove volatiles from the solids.

The experiments of temperature programmed reduction (TPR) of the catalysts (0.035 g) were carried out in a Micromeritics model TPD/TPO 2900 equipment, using a 5% H$_2$/N$_2$ mixture, from room temperature up to 1000 °C. Before the analysis, the sample was heated under nitrogen flow (60 mL min^{-1}) at 10 °C min^{-1} until 160 °C for 30 min. The hydrogen consumption in the experiments was calculated from the area under the peaks, using the calibration curve obtained with a cooper oxide (CuO) standard. The Raman spectra were obtained in a laser NRS-5100 model Jasco Raman spectrometer, using a CCD detector, a laser line of 532.13 nm and objective lens 100X, with a laser power of 1.7 mW and scanning in the range of 100–2000 nm.
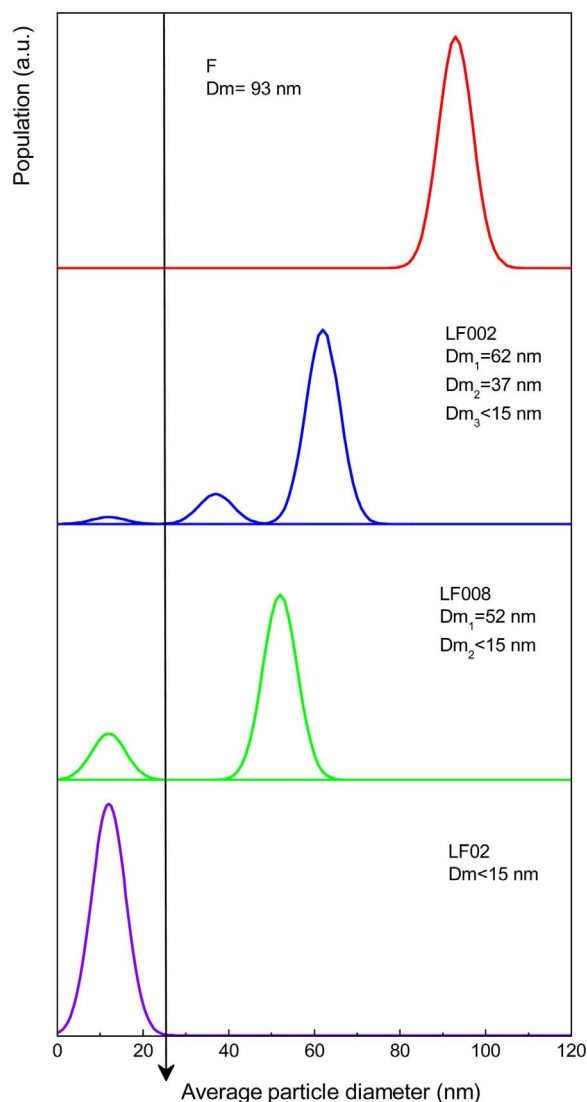
Fig. 3. Scheme of the hematite crystals size distribution as a function of lanthanum content.

During analyses, the sample was exposed to the laser for 10 s, for several times.

Mössbauer spectra were obtained in a spectrometer with 512 channels with constant acceleration and geometry of transmission. A
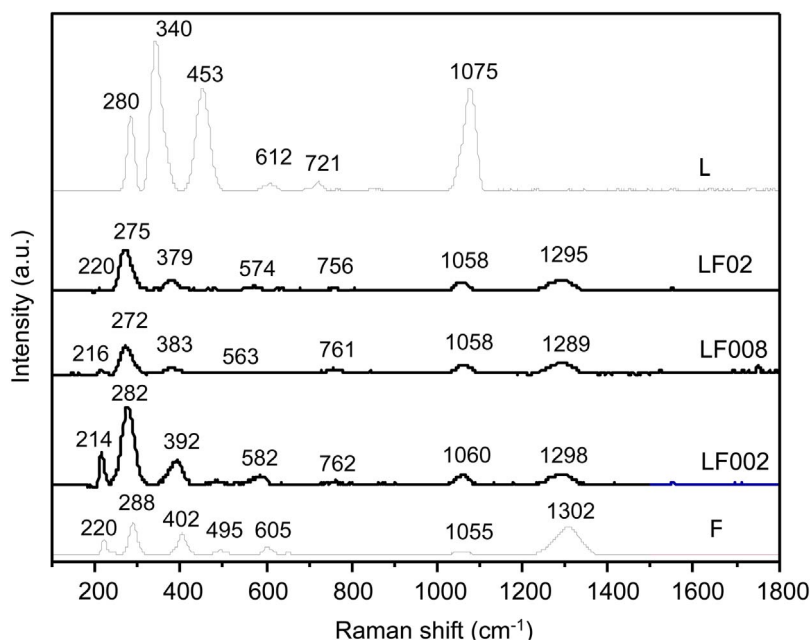
Fig. 4. Raman spectra for the catalysts.

Table 3
Specific surface areas (Sg) and average particles diameter (D) obtained by TEM for the catalysts before and after WGSR performed at 370 °C.

Sample	Sg ($m^2 g^{-1}$)	Sg^a ($m^2 g^{-1}$)	D (nm)	D^a (nm)
F	17	5.0	57	70
LF002	28	16	27	41
LF008	64	28	12	35
LF02	69	14	39	34

[a] After reaction.

source of ^{57}Co in Rh matrix of nominally 50 mCi was used. The velocity calibration was performed against a 12 μm-thick α-Fe foil. All isomer shifts (δ) mentioned in this paper are referred to this standard. For each component of the spectra, Lorentzians lines of the same width were used. The spectra were obtained at room temperature and folded to minimize geometric effects, being evaluated using a commercial computer fitting program named Recoil.

X-ray photoelectric spectroscopy measurements were performed in an electron analyzer SPECS, model Phoibos HSA-3500 150, with Al Kα radiation (1486.61 eV), pass energy of 20 eV. The powdered samples were supported on carbon double-sided tape and fixed on the XPS sample holder. The spectra were analyzed using Casa XPS software, version 2.2.99. The binding energies were referenced to the C 1s line at 284.5 eV from carbon. The curve-fittings used in the deconvolution for Fe 2p, La 3d O 1s and C 1s levels were Gaussian line shapes using the Shirley function in the background simulation. The quantitative evaluation of each peak was calculated by dividing the integrated areas under the peak by the atomic sensitivity factors considering 1.0 the sensitivity factor of C 1s (binding energy at 284.5 eV).

The transmission electron micrographs (TEM) were obtained in a Jeol JEM 1200 EXII microscope. Each catalyst was ground in an Agatha mortar and dispersed in ethanol. Diluted drops of these dispersions were placed on a 150 mesh copper grid with carbon. The micrographs were obtained in both bright and dark fields. For electron diffraction (ED) studies, 120 kV and 60 cm were used as the acceleration voltage and focus distance, respectively. Gold (Merck 99% pure) was used as a standard for calibration.

2.3. Catalyst evaluation

The catalysts were evaluated in WGSR at atmospheric pressure in the range of 150–450 °C in a tubular fixed bed microreactor (5 mm of inner diameter), under a gaseous mixture (6% CO, 10% CO_2, 25% H_2, 59% N_2) flow (135 mL min^{-1}), using a steam (30 mL/min) to carbon monoxide molar ratio of 5:1 and 160 mg of catalyst sieved in the range of 60–80 mesh to avoid diffusional limitations. The WHSV was 46.6 h^{-1}. The reaction temperature was measured by a thermocouple located in the center of the catalytic bed. Because of the small size of the reactor, it operated in isothermal mode since the radial and axial temperature profiles are negligible. The gaseous effluent was analyzed by on line gas chromatography, using a Varian Model 3800 instrument equipped with two TCD detectors. Other runs were carried out at the temperature used in the HTS step in industrial processes (370 °C), for 6 h over all catalysts. After reaction, the catalysts were characterized by X-ray diffraction, specific surface area measurements and transmission electron microscopy in order to follow the changes which might have occurred during reaction.

3. Results and discussion

The X-ray diffractograms for the fresh catalysts are shown in Fig. 1(a). As expected [20,21,29], pure iron oxide (F sample) showed the hematite (α-Fe_2O_3) pattern (JCPDS 87-1166), the same profile being displayed by the solid with the lowest amount of lanthanum (LF002 sample). For the solids with increasing lanthanum contents (LF008 and LF02 samples) the peaks were broader, indicating a decrease in the crystallites size. This effect was strongest for the lanthanum-richest solid (LF02 sample) which showed only an amorphous halo. For all cases, no phase related to lanthanum compounds (such as $FeLaO_3$ and La_2O_3) could be detected due to the coincidence of reflections of these phases with those of hematite in the diffractograms. These results are also in accordance with previous studies [13,30], in which iron oxide catalysts containing lanthanum were obtained for the synthesis of styrene.

During the water gas shift reaction, pure hematite went on phase change and the diffractograms of the spent catalyst showed only the pattern of magnetite, Fe_3O_4, (JCPDS 19-0629) as displayed in Fig. 1(b), in agreement with previous work [19–21,29]. The same profile was
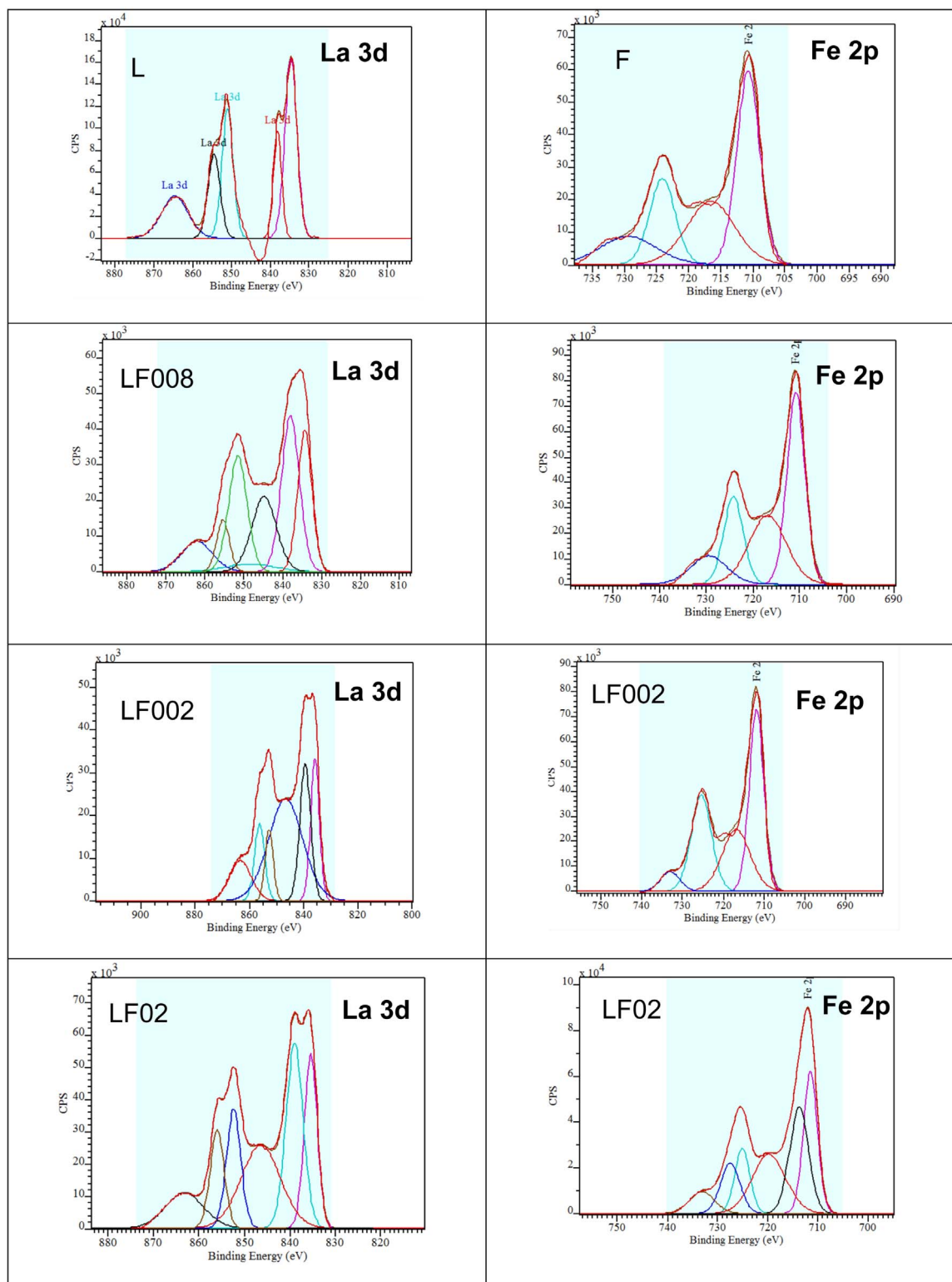
Fig. 5. X-ray photoelectron spectra for the catalysts.

noted for the lanthanum-poorest solid (LF002 sample). For the other catalysts (LF008 and LF02), the diffractograms showed broader peaks, indicating smaller crystallites size. This finding indicates that the increase of crystallites size was not significant for the samples, showing the ability of lanthanum in avoiding the sintering of iron oxide crystallites during WGSR.

In agreement with these results, pure hematite showed a Mössbauer spectrum with a sextuplet whose hyperfine parameters are typical of bulk hematite (red line), as shown in Fig. 2 and Table 1 [31,32]. Lanthanum-doped catalysts also displayed one sextet assignable to hematite (red line), whose intensity decreased when lanthanum loading increased. For the lanthanum-poorest solid (LF002 sample) a second sextuplet was included to achieve good fitting. The hyperfine parameters were also assigned to hematite (green line) but the magnetic hyperfine field markedly decreased as compared to the other one, this effect being related to magnetic collective excitations phenomenon,
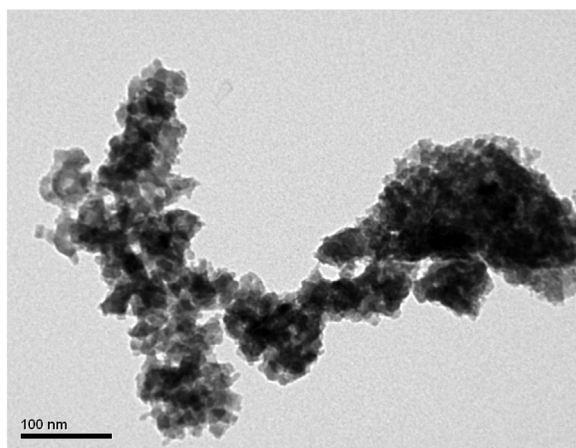
Table 4
Lanthanum to iron atomic ratio obtained by XPS analyses (± 2% error) and hydrogen consumption during TPR experiments.

Sample	La/Fe ratio	Hydrogen consumption (μmol g^{-1})
F	–	284
LF002	0.3891	330
LF008	0.3663	254
LF02	0.4132	155
L	–	27

L = lanthanum oxide.
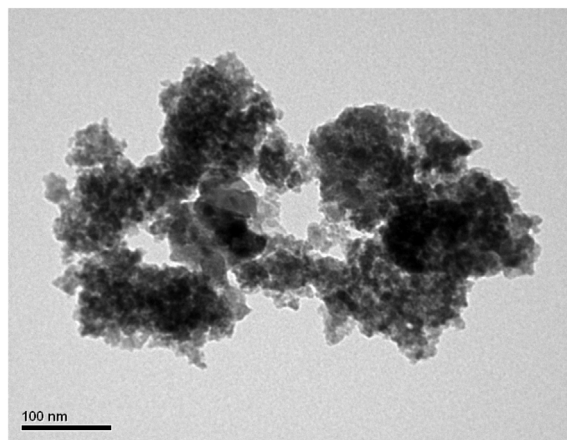
(a)

(b)

Fig. 6. Transmission electron micrographs for LF02 sample (a) before and (b) after WGSR performed ay 370 °C.

typical of magnetic small crystals [33]. For the catalyst with iron to lanthanum molar ratio of 0.08 (LF008 sample), the sextuplets disappeared and a doublet (blue line) appeared, whose intensity increased with lanthanum amount, being the only detected signal for the lanthanum-richest sample (LF02). The isomer shift of this doublet is typical of high spin Fe^{3+} ions, this being assigned to paramagnetic iron species diffused inside segregated lanthanum oxide (La_2O_3) phase and/ or superparamagnetic hematite nanoparticles.

The radius of La^{3+} species (0.105 nm) is significantly larger than the radius Fe^{3+} species (0.064 nm) and thus the possibility of La^{3+} species replace Fe^{3+} species into hematite lattice should be discarded. In addition, the production of $LaFeO_3$ perovskite should also be

discarded since their hyperfine parameters are different from that obtained for the catalysts (H = 54.6 T, $2\varepsilon = -0.085$ mm/s) [34]. Taking the previous analysis into account, we can conclude that the catalysts are made of crystals of hematite whose size decreased when lanthanum loading increased. On the other hand, the presence of Fe^{3+} ions, diffused into segregated La_2O_3 phase, cannot be discarded.

The decrease of the hyperfine magnetic field of bulk hematite allows to estimate the average crystals size of the different catalysts using the magnetic collective excitations model. For this estimation, a value of 1.4×10^3 J m^3 for basal magnetic anisotropy constant (kBu) was used. This is an appropriate value for hematite particles with average diameter larger than 20 nm [35]. The average diameters obtained following this methodology are shown in Table 2.

The crystal size distributions of hematite when lanthanum content was increased are schematized in Fig. 3. For the lanthanum-poorest catalyst (LF002 sample), the average size of the principal hematite fraction decreased from 93 to 62 nm. Besides, two new fractions with lower sizes appeared: one (magnetically blocked) with particles with 37 nm and the other one (as a minority fraction) with superparamagnetic relaxation. For the sample with La/Fe = 0.08 (LF008) the percentage of superparamagnetic fraction increased and the magnetically blocked fraction showed an average size between the two magnetic fractions present in LF002 sample. For the lanthanum-richest sample (LF02) only a superparamagnetic fraction was detected.

Fig. 4 shows the Raman spectra for the catalysts. For pure iron oxide (F sample), typical bands of hematite were observed at 220 and 495 cm^{-1}, related to A1 g modes and others at 288, 402 and 605 cm^{-1} associated with Eg modes. The band at 1302 cm^{-1} was assigned to the interaction of two magnons created by two close antiparallel spins [36]. For pure lanthanum oxide (L sample), a band 453 cm^{-1} was detected which can be related to the $E_{g\nu1}$ mode and others at 340 and 280 cm^{-1}, as observed in previous studies [37]. The bands at 721 and 1075 cm^{-1} are associated to lanthanum carbonate [37,38]. Lanthanum-doped iron oxides displayed similar spectra to hematite and lanthanum oxide, indicating the presence of both compounds in the catalysts.

The specific surface areas (Sg) of fresh and spent catalysts are shown in Table 3. One can note that lanthanum increased the specific surface area of pure iron oxide, showing its role as textural promoter. For the fresh catalysts, a progressive increase of specific surface area with lanthanum content can be noted, the maximum value being showed by the lanthanum-richest solid (LF02 sample). This can be related to the role of lanthanum in preventing the growth of iron oxide particles. These findings are in line with the results of Mössbauer spectroscopy, this textural action being mostly related to the surface, where lanthanum oxide particles are probably acting as spacers keeping iron oxide particles apart and then preventing sintering, as noted in other works [23,30].

As found by X-ray diffraction, during the water gas shift reaction, hematite changed to magnetite. For all catalysts, this phase change was followed by a sharp decrease in the specific surface area, as shown in Table 3, in accordance with previous work [8,13]. Even through, the textural action of lanthanum can still be noted for the spent catalysts.

The presence of lanthanum on the solid surface was confirmed by X-ray photoelectron spectroscopy, as shown in Fig. 5. The La 3d region was characterized by well separated spin-orbit components, La 3d5/2 and La 3d3/2, which was further splitted. The La 3d spectrum frm La_2O_3 has four visible components but only one chemical state. The surface composition of the catalysts (Table 4) showed that the relative amount of lanthanum on the solids surface was much higher than that expected in the bulk (La/Fe = 0.02, 0.08 and 0.2). However, no single relationship between the total amount of lanthanum in solids and the surface composition was found. The highest amount of lanthanum was found for LF02 sample generating the smallest particles of hematite, as concluded by the results of Mössbauer spectroscopy.

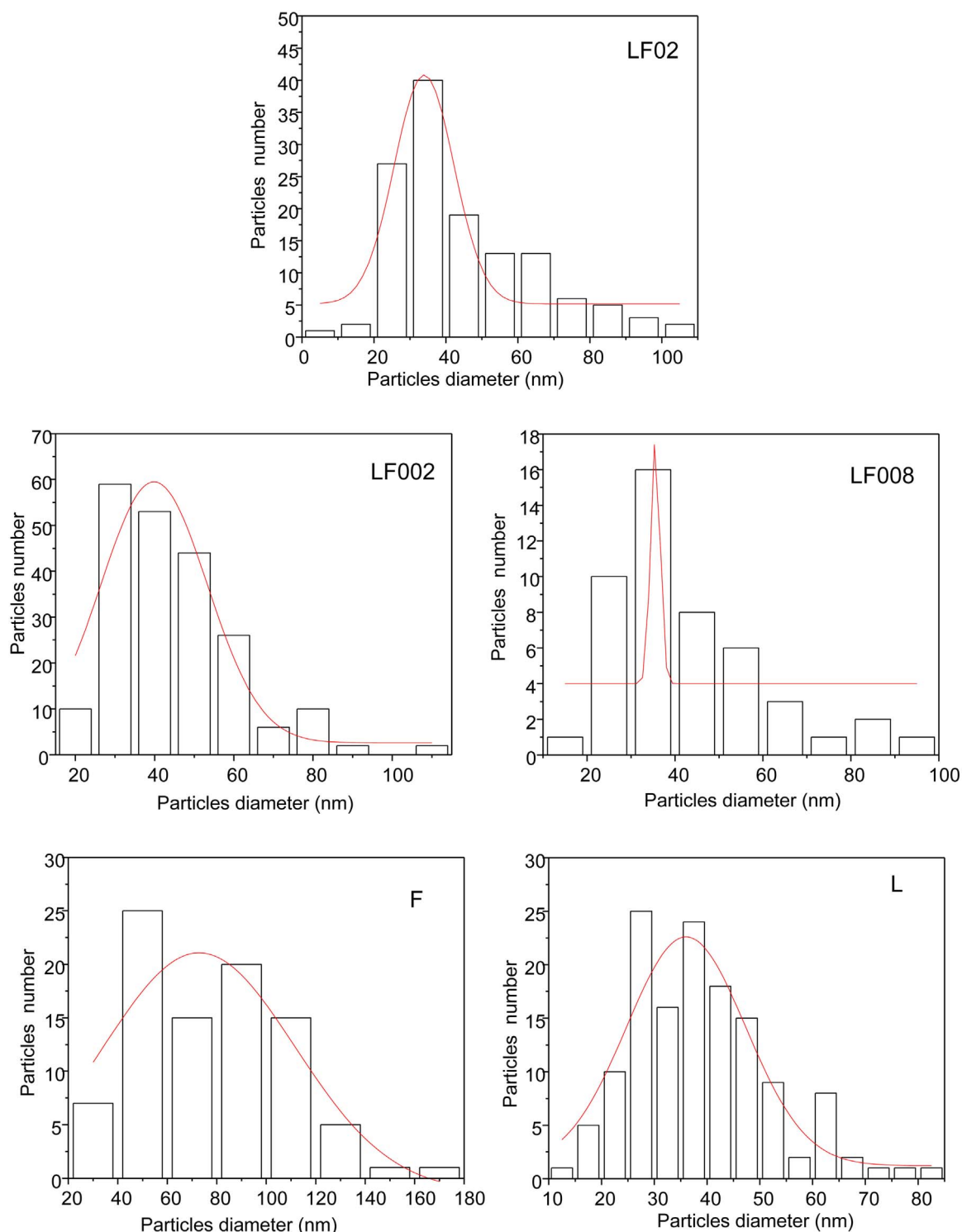The catalysts were made of aggregates of small round particles as

Fig. 7. Particles size distribution for the fresh catalysts.

illustrated in Fig. 6. By electron diffraction, it was noted that the solids were mostly bad crystallized. The average particles diameters are shown in Table 3, which shows that lanthanum decreased the particles size for both fresh and spent catalysts although no simple relationship was found between these variables. As expected, the particles size increased during WGSR, in agreement with the values of specific surface areas.

Fig. 7 shows the particles size distribution for fresh catalysts obtained by TEM. It can be noted that iron oxide (F sample) displayed broader distribution than lanthanum oxide (L sample). As the amount

of lanthanum was increased in the solids, the distribution curve was shifted to smaller sizes. A similar behavior was noted for the spent catalysts, as displayed in Fig. 8. As whole, the spent catalysts showed bigger particles than the fresh catalysts, in accordance with the values of specific surface area.

The reduction profiles of the samples are shown in Fig. 9. Pure iron oxide (F sample) showed a curve with a peak starting at 362 °C, assigned to hematite reduction to form magnetite and a broad peak beginning at 500 °C, due to magnetite reduction to produce metallic iron [20,39]. For the solid with the lowest lanthanum amount (LF002
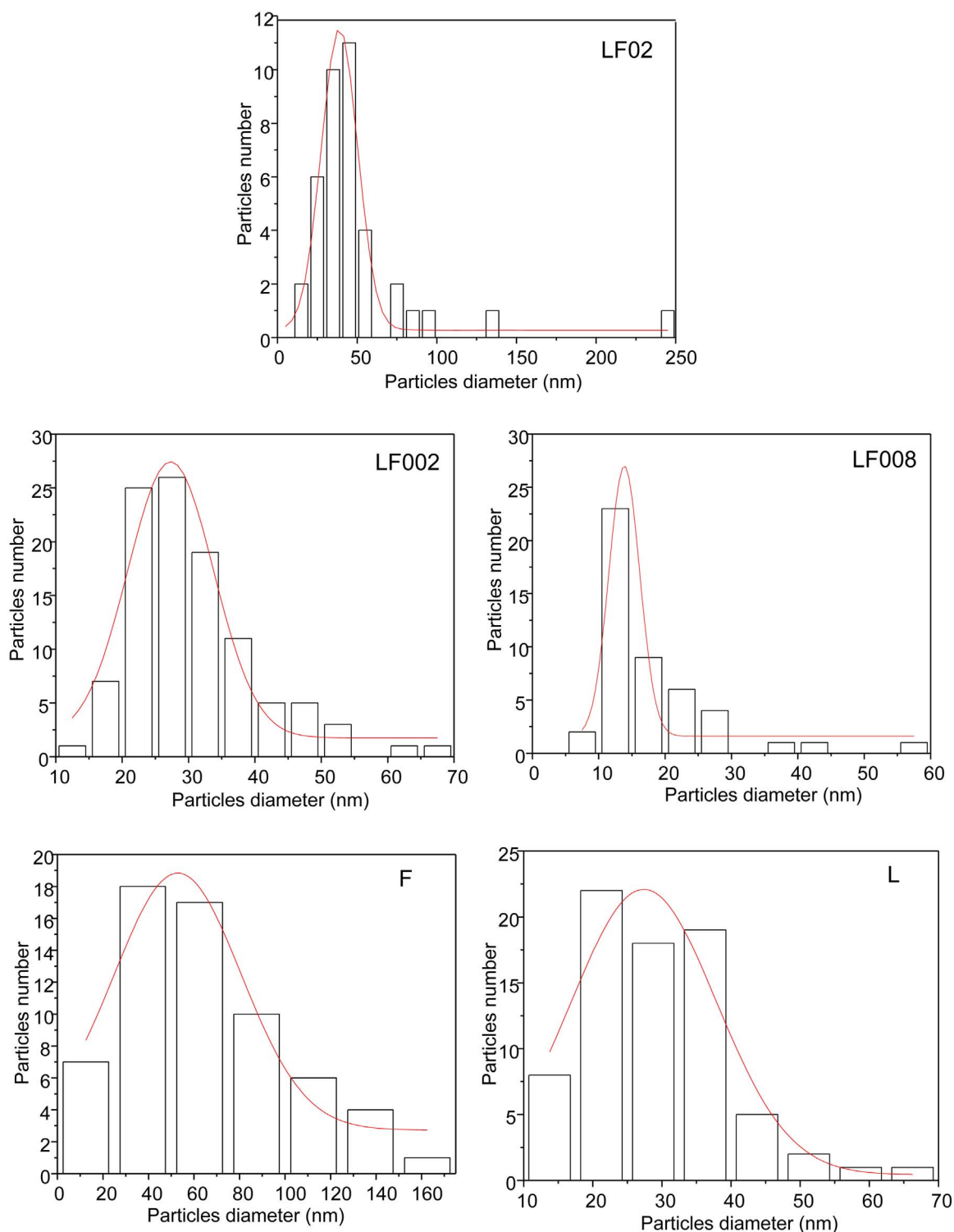
Fig. 8. Particles size distribution for the spent catalysts.

sample) the low temperature peak was shifted to higher temperatures while the high temperature peak was not affected. It means that the production of active phase of the catalyst for WGSR (magnetite) is more difficult for this sample. On the other hand, for the other solids, the low temperature peak was shifted to lower values indicating that lanthanum makes magnetite formation easier. For the high temperature peak, the highest amount of lanthanum (LF02 sample) favored magnetite reduction whereas an intermediate value (LF008 sample) did the opposite. For all lanthanum-containing samples, the high temperature peak can also be associated with the reduction of lanthanum carbonate from the

reaction of lanthanum oxide with atmospheric carbon dioxide [39].

The amount of hydrogen consumed during the TPR experiments are shown in Table 4. It can be noted that lanthanum oxide consumed very low amounts of hydrogen. In addition, lanthanum decreased the total reduction of the solids, except for the lanthanum-poorest catalyst (LF002 sample). The lowest amount of hydrogen consumed was found for the lanthanum-richest sample (LF02) probably due to the highest amount of lanthanum on the surface, making hydrogen diffusion more difficult, during the TPR experiments. From Mössbauer experiments, it was observed that some iron can be occluded inside lanthanum oxide
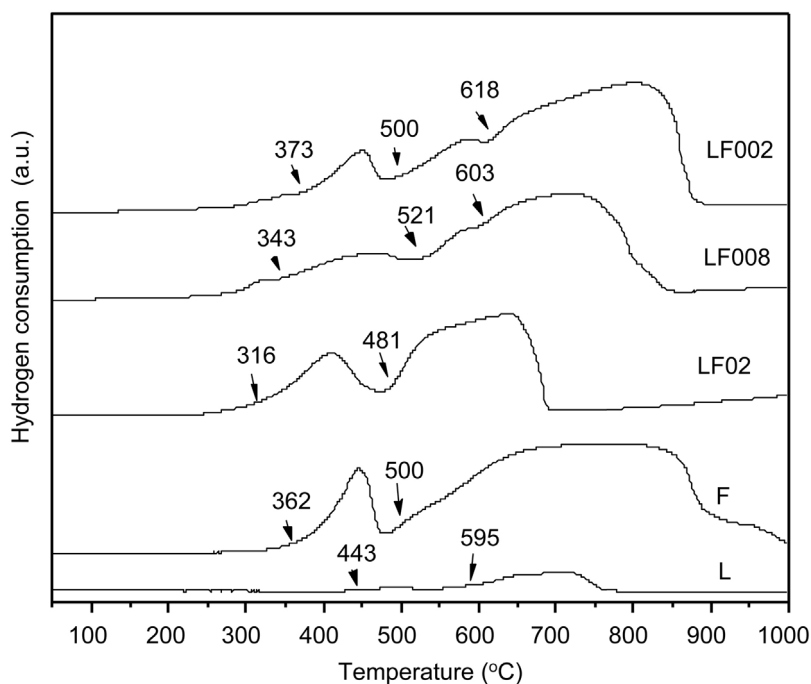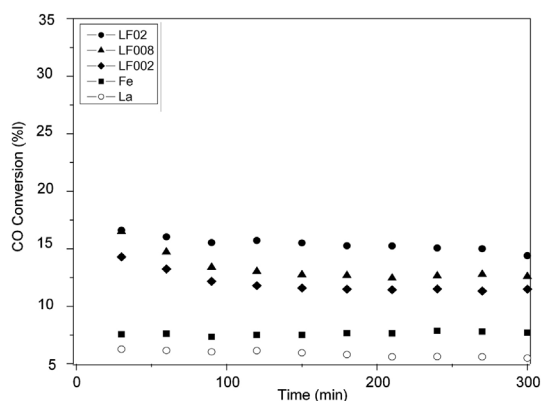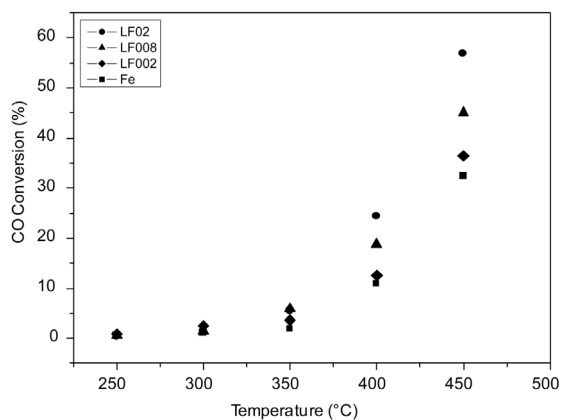
Fig. 9. Temperature programmed reduction profiles for the catalysts.

(a)

(b)

Fig. 10. Carbon monoxide conversion as a function of (a) time and of (b) temperature during WGSR performed at 370 °C.

Table 5

Carbon monoxide conversion (X_{CO}) as a function of temperature calculated by Aspen simulator.

T(°C)	X_{CO} (%)
250	96.29
300	92.12
350	85.63
370	82.38
400	76.86
450	66.26

Table 6

Catalytic activity (a), specific surface areas of spent catalysts (Sg[a]) and catalytic activity per specific surface area for the catalysts.

Sample	a × 10^5 (mol g^{-1} s^{-1})	Sg[a] (m^2 g^{-1})	a/Sg[a] × 10^7 (mol m^{-2} s^{-1})
F	0.975	5.0	5.73
LF002	1.46	16	5.20
LF008	1.59	28	2.49
LF02	1.82	14	2.64

[a] After reaction.

particles.

The values of carbon monoxide conversion obtained over the catalysts as a function of reaction time, during WGSR at 370 °C, are shown in Fig. 10(a). We can see that lanthanum oxide was almost inactive in the reaction and pure iron oxide (F sample) led to very low conversion during reaction. On the other hand, lanthanum-doped iron oxide led to higher conversions, which increased with lanthanum amounts in the solids, the LF02 sample leading to the highest values. These values are very far from the values of carbon monoxide conversion in equilibrium (Table 5). As a whole, the catalysts were stable under experimental conditions, indicating that the phase changes occurred in the first minutes of reaction. The light decrease in conversions with reaction time, probably associated with the increase of the particles size and the decrease of specific surface area during reaction. Only carbon dioxide and hydrogen were detected and no

methane or ethane was found for all catalysts, indicating that no side reaction, such as Fisher-Trospch synthesis, occurred in the reaction conditions.

Table 6 shows the activity and the activity per specific surface area for the catalysts after 6 h on stream. We can note that lanthanum increased the activity but decreased the activity per area, indicating that the iron sites were more active in lanthanum-doped iron oxides, since part of the surface was covered by lanthanum oxide. This finding can be assigned to the smallest magnetite particles, as well as to their easiness to reduction, providing more exposed active sites (magnetite) in the doped solids. It is well-known that the active phase of hematite-based catalysts is magnetite (Fe_3O_4), in which lattice the quantum jumps between the Fe^{2+} and Fe^{3+} levels in the octahedral sites enable the iron oxidation and reduction by water and carbon monoxide, respectively, during WGSR [40,41].

Fig. 10(b) shows carbon monoxide conversions as a function of temperature over the catalysts. It can be observed that all catalysts led to low values up to 300 °C, the conversions increasing with temperature, due to kinetic factors. By comparing these values with those in equilibrium (Table 5), we can see that the reaction was very far from equilibrium up to 400 °C for all catalysts. However, when the reaction was performed at 450 °C over the LF02 sample, the conversion almost reached the equilibrium value. The lanthanum-poorest catalyst (LF002 sample) led to conversions close to pure iron oxide (F sample). The other catalysts led to higher values, which increased with lanthanum content in solids.

4. Conclusions

The presence of lanthanum in hematite-based catalysts increases the specific surface area of the solids by decreasing the particles size. Lanthanum oxide remains as a segregate phase and acts as spacers on the surface, favoring the formation of small particles. In addition, lanthanum favors hematite reduction to magnetite, which is well-known as the active phase of iron oxide during the water gas shift reaction. This feature increased the activity of the catalysts in the reaction at high temperatures due to the increase in the number of exposed active sites. The solid with the highest lanthanum amount (La/Fe = 0.2) was the most active catalyst, being promising to WGSR.

Acknowledgments

References

[1] B. Viswanathan, Energy Sources (2017) 185–212.
[2] B. Viswanathan, Energy Sources (2017) 161–183.
[3] A.R. Martins, L.S. Carvalho, P. Reyes, J.M. Grau, M.C. Rangel, J. Mol. Catal. A: Chem. 429 (2016) 1–9.
[4] C. Gómez-Solís, S.L. Peralta-Arriaga, L.M. Torres-Martínez, I. Juárez-Ramírez, L.A. Díaz-Torres, Fuel 188 (2017) 197–204.
[5] D. Holladay, J. Hu, D.L. King, Y. Wang, Catal. Today 139 (2009) 244–260.
[6] P. Nikolaidis, A. Poullikkas, Renewable Sustainable Energy Rev. 67 (2017) 586–611.
[7] D.S. Newsome, Catal. Rev. Sci. Eng. 21 (1980) 275–318.
[8] J.L.R. Costa, S.G. Marchetti, M.C. Rangel, Catal. Today 77 (2002) 205–213.
[9] S.X. Wang, D. Gao, Z. Yuan, N. Liu, C. Zhang, Int. J. Hydrogen Energy 33 (2008) 3710–3718.
[10] L. Lloyd, D.E. Ridler, M.V. Twigg, The water gas shift reaction, in: M.V. Twigg (Ed.), Catalysis Handbook, Wolfe Scientific Books, London, 1996, pp. 283–339.
[11] E. Moniz, A. Meggs, G.S. MCrae, C. Ruppel, The Future of Natural Gas, An Interdisciplinary MIT Study, Cambridge, 2011.
[12] J.P. Marques, H.A. Matos, N.M.C. Oliveira, C.P. Nunes, Int. J. Hydrogen Energy 92 (2016) 376–404.
[13] M.S. Santos, S.G. Marchetti, A. Albornoz, M.C. Rangel, Catal. Today 133–135 (2008) 160–167.
[14] B. Ćosić, G. Krajačić, N. Duić, Energy 48 (2012) 80–87.
[15] B.V. Mathiesen, H. Lund, K. Karlsson, Appl. Energy 88 (2011) 488–501.
[16] G.C. Araújo, S.M. de Lima, J.M. Assaf, M.A. Peña, J.L.G. Fierro, M.C. Rangel, Catal. Today 129–135 (2008) 129–135.
[17] H. Balat, E. Kirtay, Int. J. Hydrogen Energy 35 (2010) 7416–7426.
[18] E.M. Fuentes, A.C.F. Júnior, T.F. Silva, J.M. Assaf, M.C. Rangel, Catal. Today 171 (2011) 290–296.
[19] A.L.C. Pereira, N.A. dos Santos, M.L.O. Ferreira, L.A.M. Albornoz, M.C. Rangel, Stud. Surf. Sci. Catal. 167 (2007) 225–230.
[20] G.C. Araujo, M.C. Rangel, Catal. Today 62 (2000) 201–207.
[21] A.L.C. Pereira, G.J.P. Berrocal, S.G. Marchetti, A. Albornoz, A.O. de Souza, M.C. Rangel, J. Mol. Catal. A: Chem. 281 (2008) 66–72.
[22] I. Lima Jr., J. Millet, A. Mimoun, M.C. Rangel, Appl. Catal. A: Gen. 283 (2005) 91–98.
[23] M.S. Santos, G.J.P. Berrocal, J.L.G. Fierro, M.C. Rangel, Stud. Surf. Sci. Catal. 167 (2007) 493–498.
[24] J. Tsagaroyannis, K.J. Haralambous, Z. Loizos, G. Petroutsos, N. Spyrellis, Mater. Lett. 28 (1996) 393–400.
[25] M. Laniecki, M. Ignacik, Catal. Today 116 (2006) 400–407.
[26] S. Yu Choung, M. Ferrandon, T. Krause, Catal. Today 99 (2005) 257–262.
[27] C. Wheeler, A. Jhalani, E.J. Klein, S. Tummala, L.D. Schmidt, J. Catal. 223 (2004) 191–199.
[28] A.I. Vogel, Quantitative Inorganic Analysis, Longman, London, 1961, p. 309.
[29] C.L.S. Silva, S.G. Marchetti, A. da, C. Faro Júnior, T. de, F. Silva, J.M. Assaf, M.C. Rangel, Catal. Today 213 (2013) 127–134.
[30] M. de, S. Santos, S.G. Marchetti, A. Albornoz, M.C. Rangel, Stud. Surf. Sci. Catal. 175 (2010) 819–822.
[31] E. Murad, J.H. Johnston, Iron oxides and hydroxides, in: G.J. Long (Ed.), Mössbauer Spectroscopy Applied to Inorganic Chemistry, vol. 2, Plenum Publishing Corporation, 1987, 1987.
[32] R.E. Vandenberghe, E. De Grave, C. Landuydt, L.H. Bowen, Hyperfine Interact. 53 (1990) 175–196.
[33] S. Mørup, H. Topsøe, Appl. Phys. 11 (1976) 63–66.
[34] A. Delmastro, D. Mazza, S. Ronchetti, M. Vallino, R. Spinicci, P. Brovetto, M. Salis, Mater. Sci. B Eng. 79 (2001) 140–145.
[35] F. Bødker, S. Mørup, Europhys. Lett. 52 (2) (2000) 217–223.
[36] M.A.G. Soler, F. Qu, Raman spectroscopy of iron oxide nanoparticles, in: C.S.S.R. Kumar (Ed.), Raman Spectroscopy for Nanomaterials Characterization, Springer, New York, 2012, p. 391.
[37] J. Cui, G.A. Hope, J. Spectrosc. (2015) 1–8.
[38] L.M. Cornaglia, J. Múnera, S. Irusta, E.A. Lombardo, Appl. Catal. A: Gen. 263 (2004) 91–101.
[39] H.-Y. Lin, H.Y.-W. Chen, C. Li, Therm. Acta 400 (2003) 61–67.
[40] C.H. Bartolomew, R.J. Farrauto, C.H. Bartolomew, R.J. Farrauto (Eds.), Fundamentals of Industrial Catalytic Processes, John Wiley & Sons, Hoboken NJ, 2006.
[41] C. Lund, Ind. Eng. Chem. Res. 35 (1996) 2531–2534.